

Suppression of atomic displacive excitation in photo-induced A_{1g} phonon mode of bismuth unveiled by low-temperature time-resolved x-ray diffraction

Yuya Kubota,¹ Yoshikazu Tanaka,¹ Tadashi Togashi,^{2,1} Tomio Ebisu,¹ Kenji Tamasaku,¹ Hitoshi Osawa,² Tetsuya Wada,³ Osamu Sugino,³ Iwao Matsuda,³ and Makina Yabashi^{1,2}

¹RIKEN SPring-8 Center, 1-1-1 Kouto, Sayo, Hyogo 679-5148, Japan

²Japan Synchrotron Radiation Research Institute (JASRI), 1-1-1 Kouto, Sayo, Hyogo 679-5198, Japan

³Institute for Solid State Physics, The University of Tokyo, Kashiwa, Chiba 277-8581, Japan

(*Electronic mail: kubota@spring8.or.jp)

(Dated: 1 December 2022)

An ultrafast atomic motion of a photo-induced coherent phonon of bismuth at low temperatures was directly observed with time-resolved x-ray diffraction. A cryostat with a window that is transparent to both optical lasers and x-rays enabled versatile diffraction measurements in a wide temperature range including below 10 K. It is found that an atomic displacement in a fully symmetric A_{1g} phonon mode is suppressed at low temperatures. This result indicates the displacive excitation process is suppressed in the phonon generation with decreasing temperature.

Controlling quantum phenomena in materials has been one of the central challenges in condensed matter physics. A well-promising technique is stimulating materials by external fields to excite into non-equilibrium states, where various exotic physical properties emerge. Optical pulses have been widely used as excitation sources to induce non-equilibrium quantum phenomena, such as ultrafast phase transitions, magnetic order transitions, and photo-induced superconductivities¹⁻³. Since an ultrashort pulse triggers physical events in materials before reaching the thermal equilibrium, it has opened various non-equilibrium dynamics in the quantum phases that exist only at temperatures much lower than room temperature.

Time-resolved x-ray diffraction (XRD) combined with optical pump lasers is a powerful method to investigate non-equilibrium quantum phenomena. Furthermore, x-ray free-electron lasers (XFELs)^{4,5} enable the unveiling of their ultrafast dynamics in femtosecond timescale³ such as atomic motions of photo-induced coherent phonon⁶⁻⁸. However, performing pump-probe XRD experiments has been mostly limited to a temperature range above ~ 100 K under ambient sample environments. This is because x-ray windows of standard cryostats used for low-temperature XRD, such as beryllium, carbon, and aluminum are opaque to optical lasers. Although cryostats in vacuum chambers directly connected to x-ray beamlines can achieve low temperatures below 100 K, experimental conditions are severely restricted by limitations of sample motion and 2θ angular range. A new cooling system with a suitable window material is highly required to investigate quantum phenomena under various conditions.

In this Letter, we report a notable development of the system with high versatility for pump-probe XRD at a cryogenic temperature, and direct observation of the atomic motion of bismuth (Bi) in the photo-induced coherent phonon at $T = 9$ K. Since Bi has a strong electron-lattice coupling, it has been a model material for investigating the photo-induced coherent phonon over a wide temperature range with an optical pump-optical probe (OPOP) method^{7,9-14}. However, previous

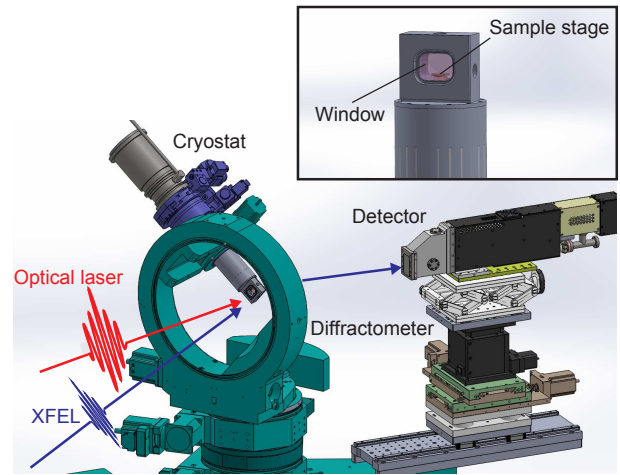


FIG. 1. Schematic of the pump-probe XRD experiment at low temperatures. A cryostat with a transparent polyimide film window is mounted on a standard four-circle diffractometer. The diffracted x-ray beam is detected with the MPCCD on the 2θ arm. The inset shows a magnified drawing of the cryostat around the sample position. A transparent polyimide film is used as a window material on the incoming side, while an aluminum-evaporated normal polyimide film, which transmits only x-rays, is used on the outgoing side.

studies have reported the atomic motion indirectly through data interpretation based on the electron-lattice interaction. Due to a lack of direct data, the issue of what process is responsible for phonon generation has remained controversial. To examine this question, it is essentially important to directly observe the lattice dynamics on a femtosecond time scale with pump-probe XRD. Our results show a suppression of the atomic displacement in the photo-induced coherent phonon at low temperatures, indicating the contribution of the displacive excitation process decreases in the phonon generation.

A pump-probe XRD experiment was performed at BL3 of

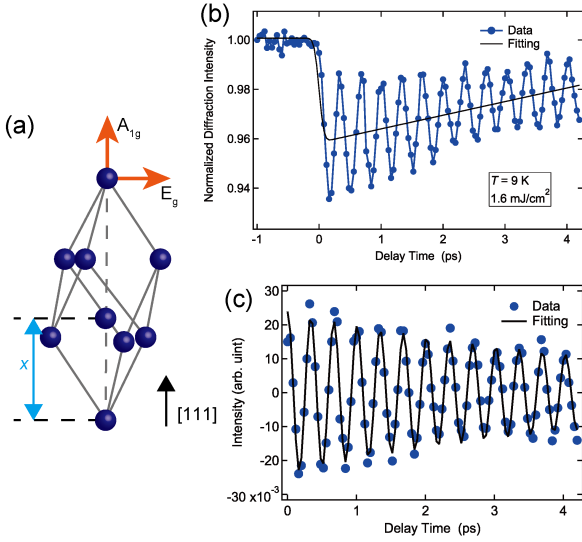


FIG. 2. (a) Structure of Bi unit cell. The blue arrow represents the length of two atomic positions, x , in a unit of the diagonal length along the $[111]$ axis. The atoms move parallel and perpendicular to the $[111]$ axis in the A_{1g} and E_g phonon modes, respectively, as shown by the orange arrows. (b) A typical result of the Bi 111 diffraction intensity variation as a function of the delay time obtained at $T = 9$ K and fluence of 1.6 mJ/cm², shown as the blue circles. The blue line is a guide to the eye. The black solid line represents a fitting curve of the non-oscillatory component with an exponential decay function convoluted with a Gaussian function. (c) Oscillatory component obtained by subtracting the non-oscillatory component from (b), shown as the blue circles. The black solid line represents a fitting exponentially decaying cosine curve.

SACLA¹⁵. Figure 1(a) shows a schematic drawing of the experimental setup. To achieve a cryogenic temperature below 100 K, we employed a highly transparent polyimide film for infrared and visible light with a thickness of 50 μm ($> 90\%$ at wavelengths above 400 nm) as a window material. It enables us a pump-probe XRD experiment at low temperatures below 10 K. The cryostat was mounted on a standard four-circle diffractometer to collect XRD signals over a wide angular range, e.g. up to ~ 100 degrees of 2θ . A 53 -nm-thick Bi film epitaxially grown on a Si (111) substrate¹⁶ was excited with 800 -nm optical laser pulses with a full-width-at-half-maximum (FWHM) duration of ~ 40 fs¹⁷. The photon energy $h\nu$ and pulse duration of the XFEL probe beam were 10 keV with a bandwidth of ~ 1 eV and ~ 7 fs (FWHM), respectively^{18–20}. The XFEL beam was focused to 100 μm in diameter (FWHM) with compound refractive lenses, while the optical laser was focused to 870 μm in diameter (FWHM). The angle between the optical laser and the XFEL beams was 1.8 degrees. The XFEL intensity of Bi 111 diffraction in a photo-excited state was detected with a multi-port charge-coupled device (MPCCD)²¹ as a function of the delay time of the XFEL pulse from the optical laser pulse. The intensity variation of Bi 111 diffraction probes the A_{1g} phonon mode oscillation along the $[111]$ direction as shown in Fig. 2(a).

Figure 2(b) shows a typical result of the Bi 111 diffraction

intensity variation as a function of the delay time (t) associated with the A_{1g} coherent phonon mode. This result was obtained at $T = 9$ K and an absorbed excitation fluence of 1.6 mJ/cm², which value was evaluated taking into account the reflectivity of 33% in the case of Bi at an incident angle of 80 degrees for p polarization in this study²². We confirmed that the lattice constant was unchanged in a time range up to at least 4 ps after a photo-excitation, judging from the position of the XRD signal observed on the MPCCD. Note that the variations of diffraction intensity represent average values over the sample thickness because the XFEL beam is almost uniformly transmitted by the 53 -nm thickness of Bi.

To obtain the information on the A_{1g} coherent phonon mode, we firstly fit the non-oscillatory component with an exponential decay function convoluted with a Gaussian function as shown by the black solid line in Fig. 2(b). We secondly obtain the oscillatory component after the subtraction of the non-oscillatory component from the total intensity variation as shown in Fig. 2(c). The frequency of photo-induced A_{1g} coherent phonon mode is 2.95 THz at $T = 9$ K and the fluence of 1.6 mJ/cm² obtained from fitting with an exponentially decaying cosine curve. This result is almost consistent with the previous OPOP study¹¹. The value of frequency is the average phonon frequency over the time range of 0 to ~ 4 ps because the chirp effect was negligible as shown in Fig. 2(c).

We measured the fluence dependence at $T = 9$ K to investigate the difference in behavior between the low and room temperatures. Figure 3(a) shows the A_{1g} phonon frequency as a function of fluence, which is compared with the published data measured at room temperature²³. Although we observed a decrease in the phonon frequency as the fluence increases at $T = 9$ K as well as at room temperature²³, the reduction at $T = 9$ K is much smaller. This behavior is consistent with the previous result obtained in the OPOP experiment¹¹.

We further investigate the atomic motion, which is inaccessible to the OPOP method, by analyzing the XRD data. The space group of Bi is #166 (R $\bar{3}m$) and its structure factor for the hkl Bragg diffraction, F_{hkl} , has the form

$$F_{hkl} = f_{\text{Bi}} \{1 + \exp[2\pi i(h+k+l)x]\} \\ = 2f_{\text{Bi}} \exp[\pi i(h+k+l)x] \cos[\pi(h+k+l)x], \quad (1)$$

where f_{Bi} is the atomic scattering factor for Bi, and x is the atomic position in the trigonal unit cell along the $[111]$ direction in a unit of the hexagonal unit-cell length, c , as shown in Fig. 2(a). The variation of the normalized 111 diffraction intensity, $I(t)/I(0)$, caused by the atomic displacement along $[111]$ direction, is represented by

$$\frac{I(t)}{I(0)} = \frac{|F_{111}(t)|^2}{|F_{111}(0)|^2} = \frac{\cos^2[3\pi x(t)]}{\cos^2[3\pi x(0)]}. \quad (2)$$

Figure 3(b) shows fluence dependence of the magnitude of the deviation of x from the equilibrium point, i.e. $\Delta x = x - x(0)$, at $T = 9$ K. The values are obtained from the minima of the fitting curves to the non-oscillatory component around $t = 0$ shown in Fig. 2(b). For the low-temperature condition, the equilibrium values of $x(0)$ and c before a photo-excitation were 0.46814 and 11.797 \AA , respectively²⁴. The

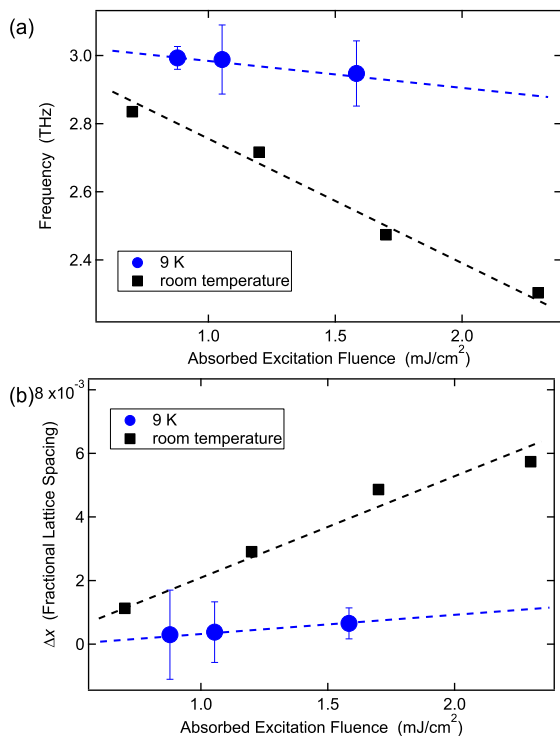


FIG. 3. (a) Frequency of the A_{1g} phonon mode of Bi obtained by fitting and (b) the atomic displacement Δx obtained from the variation of diffraction intensity around $t = 0$ at $T = 9$ K as a function of absorbed excitation fluence (blue circles), compared with those at room temperature reported by Ref.²³ (black squares). Error bars are 95% confidence intervals. The dashed lines are guides to the eye.

crystal structure of Bi is a result of Peierls distortion from a high-symmetry cubic structure. This distortion deviates x from 0.5 of the cubic structure. The decrease of the diffraction intensity shown in Fig. 2(b) indicates that quasi-equilibrium atomic position moves toward $x = 0.5$ because the 111 diffraction is forbidden for $x = 0.5$ ²³. As the fluence increases, x gradually increases toward $x = 0.5$, which implies the Peierls distortion decreases. However, the value of Δx observed at $T = 9$ K is significantly smaller than that observed at room temperature²³, as shown in Fig. 3(b). This result is consistent with the small change in the phonon frequency as the fluence increases at $T = 9$ K [Fig. 3(a)]²³. Note that we also measured the coherent phonon at room temperature with the fluence of $1.2 \text{ mJ}/\text{cm}^2$ and confirmed that the phonon frequency and Δx match with the published data²³, as shown in the supplementary material.

The time-resolved XRD observation of the small deviation Δx at $T = 9$ K provides a notable insight into the phonon-generation mechanism that has been controversial. First, we note that the deviation corresponds to the fully symmetric A_{1g} phonon mode, which has been observed predominantly at room temperature. The generation of this mode was explained by the displacive excitation of coherent phonons (DECP) model²⁵. In the DECP model, photo-excited carriers induce

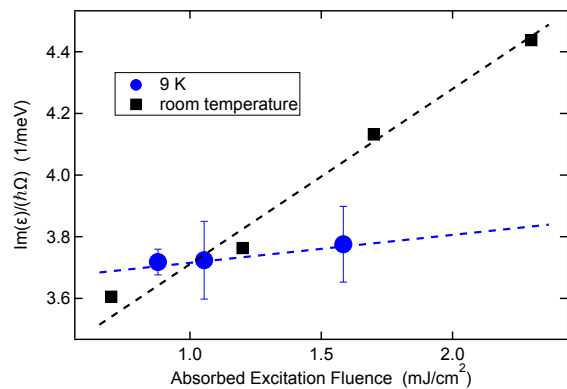


FIG. 4. $\text{Im}(\epsilon)/(\hbar\Omega)$ of the A_{1g} phonon mode of Bi as a function of absorbed excitation fluence at $T = 9$ K (blue circles) and room temperature (black squares) using the values in Fig. 3(a). The dashed lines are guides to the eye.

a shift of the equilibrium atomic position followed by atomic oscillations at the new position. In the meanwhile, there is another mode of photo-induced coherent phonon, the doubly degenerate E_g phonon mode, where atoms move in the directions perpendicular to $[111]$ [Fig. 2(a)]^{12–14,22}. The E_g phonon generation was explained by the impulsive stimulated Raman scattering (ISRS) model, where an ultrafast optical pulse having a broad energy spectrum impulsively induces stimulated Raman scattering resulting in atomic oscillations at the equilibrium position²⁶. In the literature, the E_g phonon mode was reported to be generated at low temperatures^{12–14,22}. This is ascribed to impulsive excitation, which is considered to play a more influential role as the temperature is decreased. Furthermore, the previous OPOP and spontaneous Raman scattering measurements¹⁴ concluded that the DECP and ISRS mechanisms contribute comparably even in the A_{1g} phonon mode at low temperatures.

In this context, the small value of Δx indicates that displacive excitation in the A_{1g} phonon mode is suppressed, while the contribution of the impulsive excitation becomes notable in the coherent phonon generation of Bi with decreasing temperature. Since the DECP scheme can be interpreted as the resonant case of ISRS, this transfer can be systematically theorized in terms of the Raman scattering process, as developed by Stevens *et al.*²⁷. The stimulated Raman scattering is described therein by two tensors, consisting of a common real component but different imaginary components. If the imaginary (real) part dominates, the generation mechanism of the photo-induced coherent phonon is displacive (impulsive). Therefore, one can interpret our measurement in terms of the temperature-dependent imaginary component when one assumes that the essence of photo-induced coherent phonon generation in Bi is the stimulated Raman scattering process. The imaginary component, which contributes to the displacive driving force, is proportional to $\text{Im}(\epsilon)/\Omega$, where ϵ is the dielectric function, and Ω is the phonon frequency²⁷. Figure 4 shows fluence dependence of $\text{Im}(\epsilon)/\Omega$ at $T = 9$ K and room

temperature using the values of Ω shown in Fig. 3(a). The experimental values of $\text{Im}(\epsilon)$ reported by Hunderi²⁸ were used. Although the values of $\text{Im}(\epsilon)/\Omega$ at $T = 9$ K and room temperature are comparable in the small fluence region, the values at $T = 9$ K are smaller than those at room temperature in the high fluence region (> 1 mJ/cm²). This is attributable to the fact that Ω at low temperatures is larger and its smaller change as the fluence increases than those at room temperature, as shown in Fig. 3(a) and the previous OPOP studies^{9,11,13,14}. This result indicates that high phonon frequency is equivalent to the small driving force of DECP at low temperatures, which corroborates our result of the little variation of Δx . The temperature dependence of $\text{Im}(\epsilon)/\Omega$ might be smaller than that of Δx . However, one can expect that redistribution of excitation energy from the A_{1g} to the E_g mode also contributes to the suppression of Δx from the previous report indicating that the electron-phonon coupling of the E_g phonon mode becomes stronger at low temperatures than that at room temperature¹⁴.

In conclusion, we developed a system with high versatility for pump-probe XRD at a cryogenic temperature. A cryostat with a transparent polyimide film window was mounted on a standard four-circle diffractometer, resulting in a wide acceptable range of diffraction angles even at low temperatures. We directly observed the suppression of atomic displacement in the photo-induced A_{1g} coherent phonon mode of Bi at $T = 9$ K. The result indicates that the contribution of the displacive excitation process decreases at low temperatures. It can be corroborated by the temperature dependence of the imaginary component of the tensor, which describes stimulated Raman scattering. Our experimental discovery and the phenomenological model become the research targets for the future development of theoretical studies to obtain a full understanding of the generation mechanism of the coherent phonon. This understanding will lead to the control of phonons using light, which promotes applications such as a conversion of phonon oscillations into coherent electromagnetic energy²⁹ and manipulation of atomic position and phonon to realize high- T_c superconductivities³⁰⁻³³. Our cryo-diffraction system with XFEL opens up rich avenues for unexpected discoveries and application developments in condensed matter physics.

This experiment was performed at BL3 of SACLA with the approval of the Japan Synchrotron Radiation Research Institute (JASRI) (Proposal Nos. 2018B8011, 2019A8065, 2019B8045, and 2020A8070). The synchrotron radiation experiments were performed to develop and evaluate the system at BL19LXU in SPring-8 with the approval of RIKEN (Proposal Nos. 20180094 and 20190042). We thank Dr. Suguru Ito for the sample preparation, and Dr. Jun Haruyama and Dr. Takeshi Suzuki for the valuable discussion.

SUPPLEMENTARY MATERIAL

See supplementary material for the experimental results obtained at room temperature.

AUTHOR DECLARATIONS

Conflict of Interest

The authors have no conflicts to disclose.

DATA AVAILABILITY

The data that support the findings of this study are available

from the corresponding author upon reasonable request.

- ¹K. Miyano, T. Tanaka, Y. Tomioka, and Y. Tokura, *Phys. Rev. Lett.* **78**, 4257 (1997).
- ²A. Kirilyuk, A. V. Kimel, and T. Rasing, *Rev. Mod. Phys.* **82**, 2731 (2010).
- ³M. Buzzi, M. Först, R. Mankowsky, and A. Cavalleri, *Nat. Rev. Mater.* **3**, 1 (2018).
- ⁴A. M. Kondratenko and E. L. Saldin, *Part. Accel.* **10**, 207 (1980).
- ⁵R. Bonifacio, C. Pellegrini, and L. M. Narducci, *Opt. Commun.* **50**, 373 (1984).
- ⁶K. A. Nelson, R. J. D. Miller, D. R. Lutz, and M. D. Fayer, *J. Appl. Phys.* **53**, 1144 (1982).
- ⁷T. K. Cheng, S. D. Brorson, A. S. Kazeroonian, J. S. Moodera, G. Dresselhaus, M. S. Dresselhaus, and E. P. Ippen, *Appl. Phys. Lett.* **57**, 1004 (1990).
- ⁸R. Merlin, *Solid State Commun.* **102**, 207 (1997).
- ⁹M. Hase, K. Mizoguchi, H. Harima, S. Nakashima, and K. Sakai, *Phys. Rev. B* **58**, 5448 (1998).
- ¹⁰M. Hase, M. Kitajima, S. Nakashima, and K. Mizoguchi, *Phys. Rev. Lett.* **88**, 067401 (2002).
- ¹¹O. V. Misochko, M. Hase, K. Ishioka, and M. Kitajima, *Phys. Rev. Lett.* **92**, 197401 (2004).
- ¹²O. V. Misochko, K. Ishioka, M. Hase, and M. Kitajima, *J. Phys. Condens. Matter* **18**, 10571 (2006).
- ¹³K. Ishioka, M. Kitajima, and O. V. Misochko, *J. Appl. Phys.* **100**, 093501 (2006).
- ¹⁴J. J. Li, J. Chen, D. A. Reis, S. Fahy, and R. Merlin, *Phys. Rev. Lett.* **110**, 047401 (2013).
- ¹⁵T. Ishikawa, H. Aoyagi, T. Asaka, Y. Asano, N. Azumi, T. Bizen, H. Ego, K. Fukami, T. Fukui, Y. Furukawa, S. Goto, H. Hanaki, T. Hara, T. Hasegawa, T. Hatsui, A. Higashiya, T. Hirono, N. Hosoda, M. Ishii, T. Inagaki, Y. Inubushi, T. Itoga, Y. Joti, M. Kago, T. Kameshima, H. Kimura, Y. Kirihara, A. Kiyomichi, T. Kobayashi, C. Kondo, T. Kudo, H. Maesaka, X. M. Maréchal, T. Masuda, S. Matsubara, T. Matsumoto, T. Matsushita, S. Matsui, M. Nagasono, N. Nariyama, H. Ohashi, T. Ohata, T. Ohshima, S. Ono, Y. Otake, C. Saji, T. Sakurai, T. Sato, K. Sawada, T. Seike, K. Shirasawa, T. Sugimoto, S. Suzuki, S. Takahashi, H. Takebe, K. Takeshita, K. Tamasaku, H. Tanaka, R. Tanaka, T. Tanaka, T. Togashi, K. Togawa, A. Tokuhisa, H. Tomizawa, K. Tono, S. Wu, M. Yabashi, M. Yamaga, A. Yamashita, K. Yanagida, C. Zhang, T. Shintake, H. Kitamura, and N. Kumagai, *Nat. Photonics* **6**, 540 (2012).
- ¹⁶M. Kammmler and M. Horn-Von Hoegen, *Surf. Sci.* **76**, 56 (2005).
- ¹⁷T. Togashi, S. Owada, Y. Kubota, K. Sueda, T. Katayama, H. Tomizawa, T. Yabuuchi, K. Tono, and M. Yabashi, *Appl. Sci.* **10**, 7934 (2020).
- ¹⁸Y. Inubushi, K. Tono, T. Togashi, T. Sato, T. Hatsui, T. Kameshima, K. Togawa, T. Hara, T. Tanaka, H. Tanaka, T. Ishikawa, and M. Yabashi, *Phys. Rev. Lett.* **109**, 144801 (2012).
- ¹⁹Y. Inubushi, I. Inoue, J. Kim, A. Nishihara, S. Matsuyama, H. Yumoto, T. Koyama, K. Tono, H. Ohashi, K. Yamauchi, and M. Yabashi, *Appl. Sci.* **7**, 584 (2017).
- ²⁰I. Inoue, T. Hara, Y. Inubushi, K. Tono, T. Inagaki, T. Katayama, Y. Amemiya, H. Tanaka, and M. Yabashi, *Phys. Rev. Accel. Beams* **21**, 080704 (2018).
- ²¹T. Kameshima, S. Ono, T. Kudo, K. Ozaki, Y. Kirihara, K. Kobayashi, Y. Inubushi, M. Yabashi, T. Horigome, A. Holland, K. Holland, D. Burt, H. Murao, and T. Hatsui, *Rev. Sci. Instrum.* **85**, 033110 (2014).
- ²²S. L. Johnson, P. Beaud, E. Möhr-Vorobeva, A. Caviezel, G. Ingold, and C. J. Milne, *Phys. Rev. B* **87**, 054301 (2013).
- ²³D. M. Fritz, D. A. Reis, B. Adams, R. A. Akre, J. Arthur, C. Blome, P. H. Bucksbaum, A. L. Cavalieri, S. Engemann, S. Fahy, R. W. Falcone, P. H. Fuoss, K. J. Gaffney, M. J. George, J. Hajdu, M. P. Hertlein, P. B. Hillyard, M. Horn-von Hoegen, M. Kammmler, J. Kaspar, R. Kienberger, P. Krejčík, S. H. Lee, A. M. Lindenberg, B. McFarland, D. Meyer, T. Montagne, Å.L. D. Murray, A. J. Nelson, M. Nicoul, R. Pahl, J. Rudati, H. Schlarb, D. P. Siddons, K. Sokolowski-Tinten, T. Tschemtscher, D. von der Linde, and J. B. Hastings, *Science* **315**, 633 (2007).
- ²⁴P. Cucka and C. S. Barrett, *Acta Crystallogr.* **15**, 865 (1962).
- ²⁵H. J. Zeiger, J. Vidal, T. K. Cheng, E. P. Ippen, G. Dresselhaus, and M. S. Dresselhaus, *Phys. Rev. B* **45**, 768 (1992).
- ²⁶Y. X. Yan, E. B. Gamble, and K. A. Nelson, *J. Chem. Phys.* **83**, 5391 (1985).

- ²⁷T. E. Stevens, J. Kuhl, and R. Merlin, *Phys. Rev. B* **65**, 144304 (2002).
- ²⁸O. Hunderi, *J. Phys. F Met. Phys.* **5**, 2214 (1975).
- ²⁹T. Dekorsy, H. Auer, C. Waschke, H. J. Bakker, H. G. Roskos, H. Kurz, V. Wagner, and P. Grosse, *Phys. Rev. Lett.* **74**, 738 (1995).
- ³⁰K. Okazaki, H. Suzuki, T. Suzuki, T. Yamamoto, T. Someya, Y. Ogawa, M. Okada, M. Fujisawa, T. Kanai, N. Ishii, J. Itatani, M. Nakajima, H. Eisaki, A. Fujimori, and S. Shin, *Phys. Rev. B* **97**, 121107(R) (2018).
- ³¹S. Gerber, S.-L. Yang, D. Zhu, H. Soifer, J. A. Sobota, S. Rebec, J. J. Lee, T. Jia, B. Moritz, C. Jia, A. Gauthier, Y. Li, D. Leuenberger, Y. Zhang, L. Chaix, W. Li, H. Jang, J.-S. Lee, M. Yi, G. L. Dakovski, S. Song, J. M. Glownia, S. Nelson, K. W. Kim, Y.-D. Chuang, Z. Hussain, R. G. Moore, T. P. Devereaux, W.-S. Lee, P. S. Kirchmann, and Z.-X. Shen, *Science* **357**, 71 (2017).
- ³²T. Suzuki, T. Someya, T. Hashimoto, S. Michimae, M. Watanabe, M. Fujisawa, T. Kanai, N. Ishii, J. Itatani, S. Kasahara, Y. Matsuda, T. Shibauchi, K. Okazaki, and S. Shin, *Commun. Phys.* **2**, 115 (2019).
- ³³R. Mankowsky, A. Subedi, M. Först, S. O. Mariager, M. Chollet, H. T. Lemke, J. S. Robinson, J. M. Glownia, M. P. Minitti, A. Frano, M. Fechner, N. A. Spaldin, T. Loew, B. Keimer, A. Georges, and A. Cavalleri, *Nature* **516**, 71 (2014).